Novel Geometric Morphometric Analysis for Application in Evaluating Chiari I Malformations

Perera, I., Moriarty, S., Simmons, Z., Mahoney, M., Malek, Z., Botkin, C., Millard J.A., Department of Biomedical Sciences, Edward Via College of Osteopathic Medicine, Blacksburg, VA, 24060, USA

Introduction and Objectives

Type I Chiari malformations (CMI) are caudal displacements of the cerebellar tonsils through the foramen magnum (**Fig.1**). Additional structural abnormalities include ventral flattening of the midbrain, pons, and medulla. 50-75% of CMI patients will also present with a syrinx in the lower cervical or upper thoracic spinal cord. Rarely, CMI may accompany hydrocephalus. The current accepted diagnosis of CMI is tonsillar herniation greater than 5mm below the foramen magnum (**Fig.2**) (Hiremath, 2020). Diagnosis of CMI is made by cross-sectional imaging and measurement of the position of the cerebellar tonsils. While volumetric CT scanning can be informative, the preferred imaging modality for assessing CMI is MRI (Gaillard, 2023). The primary aims of this research are:

- Develop a reliable 3-D landmarking protocol using Chiari malformation medical imaging to test hypotheses which aim to effectively discriminate between Chiari patients and non-Chiari individuals.
- Measure, quantify, and describe the shape variation (and potential covariations) seen in Chiari patients.
- Identify anatomical shape locales which further elucidate disease etiology.
- Determine the consistency of landmarking investigators via analysis of variance in Procrustes distance (Error Study)

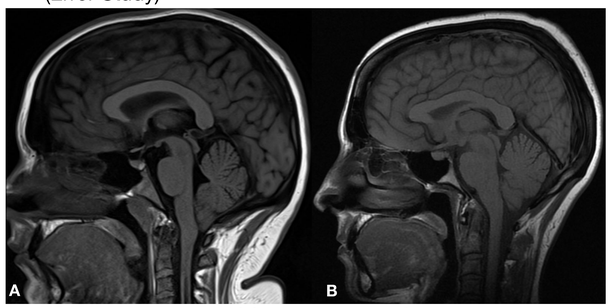

Figure 1. Midsagittal MRIs of **(A)** an individual with CMI and a syrinx and **(B)** a healthy individual.

Figure 2. Radiologic evaluation of tonsillar ectopia.(Gaillard, 2023).

Materials and Methods

- Midsagittal MRI images from 94 Chiari-affected females and matched controls were landmarked using tpsDig264 (v.2.32) and tpsUtil64 (v.1.82) (SUNYmorph) (**Table1**).
- A total of 10 discrete and 155 semilandmarks were placed on features of the midbrain and hindbrain (**Fig.3**).
- MorphoJ (v1.07a) and Past (v4.03) were used to perform a generalized Procrustes superimposition and principal component analysis (PCA). Independent-samples t-tests were applied to principal component (PC) scores to evaluate hypotheses related to configurational differences between groups.
- To evaluate replicability of the landmarking protocol, five researchers landmarked 10 replicates. The variance for each individual landmark was assessed by computing the average Procrustes distance between the mean landmark position and each individual replicate for each researcher.

Table 1. Discrete Landmarks with Definitions.

Landmark	Definition
Ventral spinal cord	Ventral spinal cord at the point of its axial intersection with the C2/3 intervertebral disc
Pontomedullary junction	Point where medulla oblongata meets pons
Pontomesencephalic junction	Point where midbrain meets pons
Ventral tegmental area	Anterior-superior-most visible point on the midbrain
Cerebral aqueduct #1	Superior-most point of aqueduct bound by tectum and tegmentum
Cerebral aqueduct #2	Inferior-most point of aqueduct bound by tectum and tegmentum
Dorsal spinal cord	Ventral spinal cord at the point of its axial intersection with the C2/3 intervertebral disc
Anterior cerebellar lobe	Point where anterior lobe of cerebellum meets the superior medullary velum
Primary cerebellar fissure	Deepest visible point of the primary cerebellar fissure
4th ventricle	Posterior-most point of the roof of the 4th ventricle superior to the nodulus
Ventral spinal cord	Ventral spinal cord at the point of its axial intersection with the C2/3 intervertebral disc

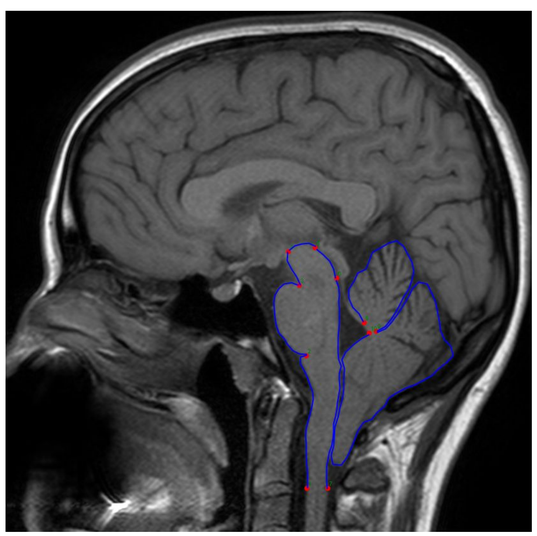

Figure 3. Midsagittal view with all discrete and semilandmarks visible.

Results

PCA revealed 93 loadings with the first four accounting for 65.126% of the overall variation in the shape. The scatterplots contain 95% confidence ellipses for the mean. The first PC indicated inferior displacement of the cerebellar tonsils, posterior displacement of the posterior cerebellar lobe and 4th ventricle with concomitant ventral migration of the midbrain, and dorsal migration of the medulla. Mean scores along PC1 were significantly different between affected and control groups ($t(93) = 6.8$, $p < 0.001$) (**Figs.4&5**). In an affected-only analysis, mean shape conformation did not effectively discriminate between individuals with a history of syringomyelia and those without (**Fig.6**). There was a significant difference along PC2 for individuals receiving a diagnosis under age 30 versus those over age 30 ($t(65) = 2.4$, $p = 0.017$). There was a small amount of variation in the average Procrustes distances between replicates among individual landmarkers (**Fig.7**). No trends in problematic landmark variability were detected.

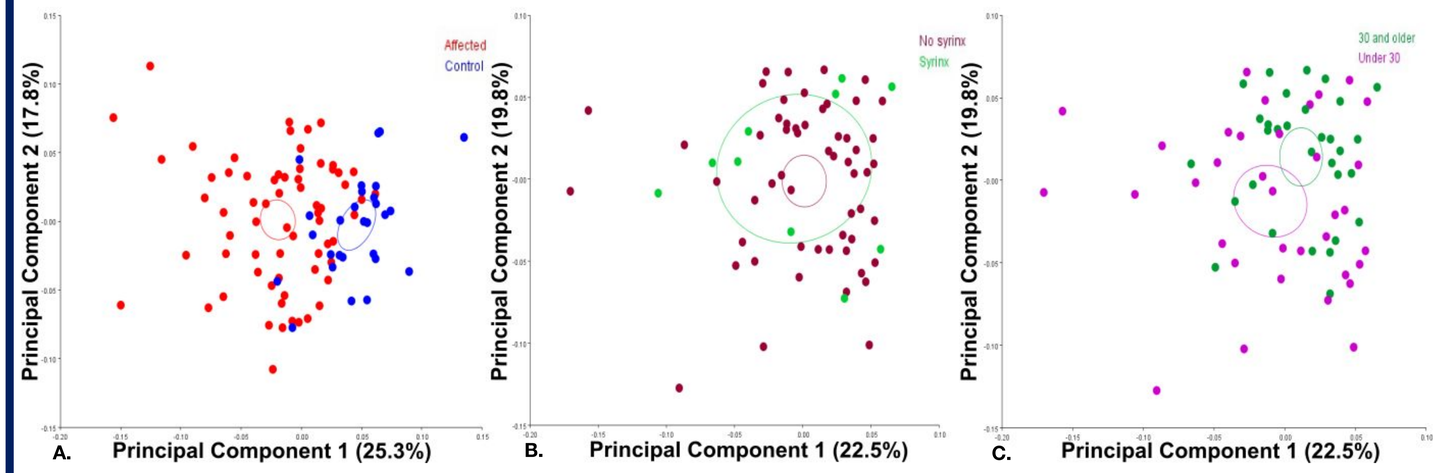

Figure 4. PC1 vs. PC2 Scatterplots. **(A)** All Individuals, both affected and control. **(B)** Affected Only, Syrinx vs. No syrinx. **(C)** Affected Only, diagnosis over age 30 vs. under age 30.

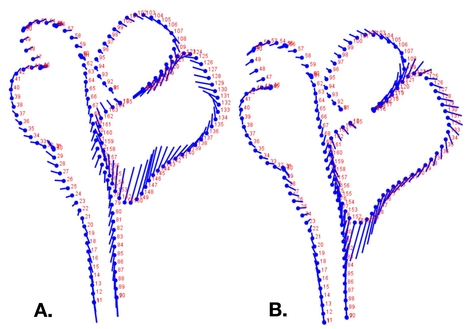

Figure 5. Lollipop Diagrams of entire sample along PC1. **(A)** Scale Factor +0.15 (extreme control). **(B)** Scale Factor -0.15 (extreme Chiari).

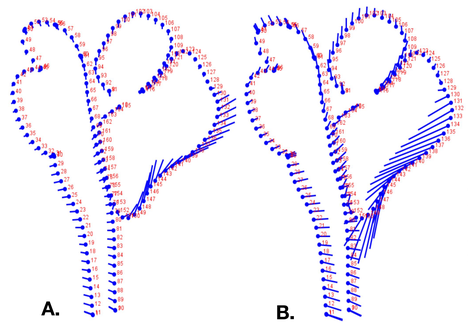

Figure 6. Lollipop diagrams of affected-only analysis along PC2. **(A)** Scale Factor +0.1. **(B)** Scale Factor -0.15.

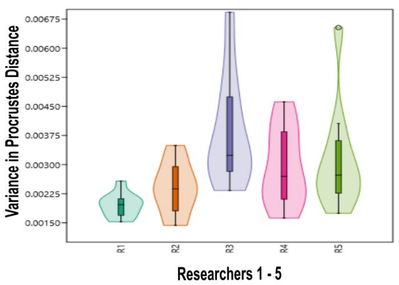

Figure 7. Box plot (with violin) demonstrating the variance among landmarking researchers in the error study.

Conclusions

Geometric analysis effectively discriminates between Chiari-affected individuals and matched controls. Aside from predictably highlighting tonsillar ectopia, results demonstrated numerous additional anatomical conformations in individuals with Chiari I malformation, including coronal tilting of the brainstem's overall conformation, resulting in a more dorsally positioned medulla and ventrally positioned midbrain. Also, sagging of the inferior medullary velum was notable in Chiari-affected individuals. Interestingly, shape conformation does not appear to differ between individuals with a history of syringomyelia and those without. These subtle shape conformations would be exceedingly difficult to detect without statistical shape analysis. Future directions should include machine learning to evaluate subtle shape differences between groups with the goal of integrating results into clinical decision-making.

Acknowledgements

This research protocol was approved by the VCOM IRB (2022-049) and funded by the Edward Via College of Osteopathic Medicine Research Eureka Accelerator Program (REAP). The researchers would like to extend our gratitude to the Conquer Chiari Research Program and the University of Akron for supplying data from the Chiari1000 research effort and for their continued collaboration in this effort.

References and E-copy of Poster